EEET ECOLOGICAL ENGINEERING & ENVIRONMENTAL TECHNOLOGY

Ecological Engineering & Environmental Technology, 2026, 27(6), 322–341
https://doi.org/10.12912/27197050/221579
ISSN 2719–7050, License CC-BY 4.0

Received: 2026.04.21
Accepted: 2026.05.18
Published: 2026.06.01

Satellite-based estimation of PM_{10} concentrations with ground validation using multiple linear regression in Makassar, Indonesia

Muh. Khalil Jibran[1], Sumarni Hamid Aly[1*], Muralia Hustim[1], Nurul Masyiah Rani Harusi[1], Muhammad Rizieq Akbar Mubarak[1], Alisyah Ismi Zahra Mardan[1]

[1] Department of Environment Engineering, Faculty of Engineering, University of Hasanuddin, Malino St. km 6, Gowa Regency, Sulawesi Selatan, 92171, Indonesia
* Corresponding author's e-mail: marni_hamidaly@yahoo.com

ABSTRACT

This study estimates and maps PM_{10} concentrations in Makassar, Indonesia, using Landsat 8 imagery integrated with field-based measurements, and evaluates whether multi-band spectral information improves satellite-based PM_{10} estimation in a tropical coastal urban environment. Landsat 8 OLI/TIRS Collection 2 Level-1 imagery acquired on 27 March 2025 was processed through radiometric correction, atmospheric correction, and spectral reflectance extraction. Field-based PM_{10} measurements were collected from 30 observation points using the gravimetric method. The dataset was divided into 80% for model development and 20% for independent validation. Landsat 8 Bands 1–4 were used as predictor variables in multiple linear regression models, and model performance was evaluated using the correlation coefficient, coefficient of determination, and root mean square error. The results showed that Bands 1–4 had significant positive correlations with PM_{10} concentrations, with correlation coefficients ranging from 0.709 to 0.755. Model B, which combined Bands 1, 2, 3, and 4, produced the best performance, with $R = 0.811$ and $R^2 = 0.658$ during model development. Independent validation confirmed its superior performance, with $R = 0.781$, $R^2 = 0.609$, and RMSE = 33.1083 μg/m³. These findings indicate that satellite-based PM_{10} estimation in Makassar is feasible, but should be interpreted as a spatial approximation rather than a direct replacement for ground-based measurements. The model remains affected by optical sensor limitations, temporal differences between image acquisition and field measurements, cloud-related constraints, and the absence of meteorological variables. Practically, the resulting PM_{10} maps can help identify priority areas for air quality monitoring in cities with limited monitoring infrastructure. The originality of this study lies in demonstrating that a multi-band Landsat 8 configuration is more suitable for representing PM_{10} variability in a medium-sized tropical coastal city by capturing aerosol scattering, heterogeneous urban surfaces, and coastal environmental influences.

Keywords: PM_{10} estimation, satellite imagery, air quality modeling, multiple linear regression, urban air pollution.

INTRODUCTION

Air quality is one of the primary indicators of urban environmental health and public well-being. In recent decades, air pollution has evolved into an increasingly serious global issue. The World Health Organization (WHO) reports that approximately 99% of the global population is still exposed to air that does not meet health-based quality standards, with ambient air pollution causing more than seven million premature deaths each year (Shaddick et al., 2020; WHO, 2021). This condition is closely associated with the growing pressure of anthropogenic activities on the atmosphere, particularly in urban areas.

In urban regions, population growth, high mobility, and rapid infrastructure development contribute to increasing emissions from the transportation sector, fossil fuel–based energy consumption, as well as industrial and construction

activities (Thanvisitthpon et al., 2024). These activities contribute to elevated concentrations of air pollutants, particularly suspended particulate matter. Furthermore, the physical characteristics of cities, such as high building density and limited green open spaces, often restrict natural air circulation, thereby increasing the potential accumulation of pollutants in the lower layers of the atmosphere (Bernardino et al., 2021). Therefore, the dynamics of urban air quality are influenced by a combination of emission sources and the spatial structure of the city (Han et al., 2020).

One of the most dominant and persistent air pollutants in urban areas is particulate matter with an aerodynamic diameter of less than 10 µm (PM10). These fine particles have the potential to penetrate the human respiratory system and cause various adverse health effects. PM_{10} concentrations in many major cities across Asia, including Indonesia, are frequently reported to exceed the annual guideline value established by the WHO, which is 15 µg/m³. For instance, the cities of Jakarta and Surabaya record PM_{10} concentrations of approximately 40–60 µg/m³ (KLHK, 2023), while Bangkok, Hanoi, and Manila show concentrations ranging from 40 to 90 µg/m³ (Usman, 2023; Santoso et al., 2021; Phan et al., 2020).

Makassar, one of the major economic growth centers in eastern Indonesia, is experiencing a similar challenge. Population growth, increased transportation activities, and the expansion of built-up areas have the potential to elevate particulate emissions into the atmosphere. Data from Ministry of Environment and Forestry of Indonesia (KLHK, 2023) indicate that PM_{10} concentrations in Makassar periodically range between 50 and 60 µg/m³, suggesting a level of air pollution that requires serious attention.

However, the air quality monitoring system in Makassar still faces significant limitations, particularly in terms of the number and spatial distribution of monitoring stations. According to data from IQAir (2024–2025), South Sulawesi Province has only three air quality monitoring stations, with only one located in Makassar. This condition results in spatially limited PM_{10} measurement data, making it difficult to comprehensively represent the spatial distribution of air pollution across the city.

The limitations of terrestrial monitoring data highlight the need for alternative approaches in air quality assessment. In this context, satellite-based remote sensing technology offers considerable potential for estimating air quality parameters both spatially and temporally, as it provides broad and consistent spatial coverage that can complement the limitations of ground-based measurements (Ranjan et al., 2021). Several previous studies have also utilized remote sensing data to analyze urban air quality. For example, the integration of Landsat 8 and MODIS imagery has been applied to estimate atmospheric pollutant concentrations, revealing seasonal variations in air pollution across the metropolitan area of Makassar (Harusi et al., 2025). These findings demonstrate the potential of satellite imagery for monitoring urban air quality.

Landsat 8 is one of the most widely used remote sensing platforms in urban environmental studies, including research related to air quality. The satellite is equipped with the operational land imager (OLI) and thermal infrared sensor (TIRS), which capture multispectral data across various wavelengths with relatively high spatial resolution, making them suitable for environmental analysis at the urban scale (Small and Zappa, 2017). These characteristics make Landsat 8 particularly relevant for urban environments that exhibit diverse land-use patterns and high intensities of human activities.

Several studies indicate that spectral reflectance recorded by the OLI sensor, particularly within the visible to shortwave infrared spectrum, is associated with the presence of atmospheric particulates (Yang et al., 2021). Suspended particles such as PM_{10} influence the scattering and absorption processes of electromagnetic radiation, meaning that variations in their concentrations can be reflected in changes in satellite image reflectance values (Fernández-Pacheco et al., 2018). Based on this mechanism, spectral parameters derived from Landsat 8 have frequently been used as predictor variables in the development of empirical PM_{10} models through statistical and regression-based approaches (Heriza et al., 2023).

PM_{10} modeling approaches based on Landsat 8 have been applied in various urban regions and have demonstrated a relatively good capability in representing the spatial variability of particulate concentrations, particularly when calibrated with ground-based measurement data (Liu and Wang, 2024). The advantages of Landsat 8 in terms of long-term data availability and wide spatial coverage make it an important alternative in regions with limited air quality monitoring stations (Lin et al., 2021). Nevertheless, several studies

emphasize that the success of PM_{10} estimation strongly depends on the quality of image preprocessing, including radiometric and atmospheric corrections, as well as the suitability of statistical models to the local characteristics of the study area (Ranjan et al., 2021). However, most of these studies have primarily focused on major metropolitan areas worldwide, while investigations in medium-sized developing cities such as Makassar remain relatively limited.

Although satellite-based PM_{10} estimation has shown promising results, several research gaps remain. Most previous studies have focused on large metropolitan areas with more extensive monitoring infrastructure, while medium-sized tropical coastal cities remain underrepresented. In addition, the spectral sensitivity of Landsat 8 bands to particulate matter concentrations under tropical coastal atmospheric conditions has not been sufficiently evaluated using field-based validation data. Previous studies have shown that satellite-based particulate matter estimation is strongly influenced by aerosol data quality, model selection, atmospheric correction, and local environmental conditions (Ranjan et al., 2021; Heriza et al., 2023; Lin et al., 2021).

In Indonesia, air quality studies are still dominated by monitoring-station-based approaches, whereas remote sensing applications remain limited. Satellite-based air quality assessment has been applied in Makassar, but previous work has mainly focused on seasonal pollutant estimation using Landsat 8 and MODIS rather than field-validated PM_{10} estimation using Landsat 8 spectral bands (Harusi et al., 2025). Therefore, the spatial distribution of PM_{10} and the predictive capability of Landsat 8 spectral bands in Makassar remain insufficiently understood.

Therefore, this study aims to develop and validate a Landsat 8–based multiple linear regression model for estimating PM_{10} concentrations in Makassar and to evaluate its spatial predictive performance using ground-based measurements. This study also seeks to determine whether the integration of Band 1 as a coastal/aerosol band with visible Bands 2–4 can provide a stronger empirical representation of PM_{10} variability in a tropical coastal urban environment. This study contributes to filling the knowledge gap in satellite-based PM_{10} estimation for medium-sized tropical coastal cities with limited monitoring infrastructure.

This study is based on three hypotheses: Landsat 8 spectral bands are significantly correlated with PM_{10} concentrations; multi-band regression models provide higher predictive performance than more limited band combinations; and aerosol-sensitive bands contribute to PM_{10} estimation performance when integrated with other visible bands. The findings are expected to support satellite-based air quality monitoring, spatial pollution assessment, and urban environmental management in rapidly growing coastal cities.

METHODOLOGY

Study area

This study was conducted in Makassar due to its status as a rapidly developing urban center and the capital city of South Sulawesi Province, Indonesia. Geographically, the city is located between 119°4′29.038″–119°32′35.781″ East Longitude and 4°58′30.052″–5°14′0.146″ South Latitude. Administratively, Makassar covers an area of approximately 175.77 km² and is divided into 15 districts comprising 153 urban villages. As a major urban center experiencing intensive development, Makassar faces increasing anthropogenic pressures that contribute to air pollution, particularly particulate matter. Urban dynamics, high population density, and expanding transportation and industrial activities make Makassar an ideal case study for satellite-based air quality modeling (Figure 1).

Dataset and methods

This study applied a quantitative modeling approach to estimate PM_{10} concentration using Landsat 8 imagery and field measurements in Makassar City. Spectral reflectance variables extracted from Landsat 8 imagery were integrated with PM_{10} concentration data obtained from 30 field observation points distributed across various urban areas. A total of 30 observation points were divided into training and testing subsets. The PM_{10} observation dataset was divided into model development and validation subsets. Twenty-four samples (80%) were used for regression model development, while six samples (20%) were reserved for independent validation. Twenty-four samples (80%) were used for regression model development, while six samples (20%) were reserved for independent validation. This data partitioning followed a fixed hold-out validation approach. Cross-validation was not applied due to

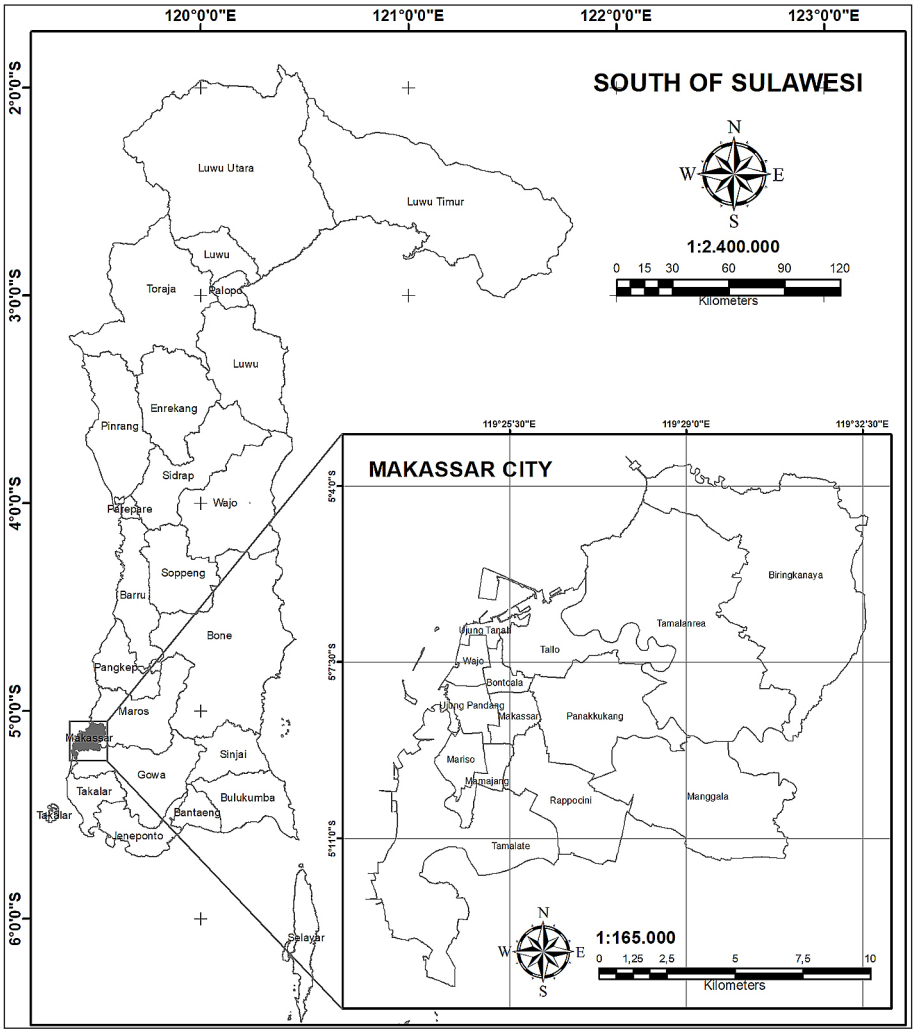

Figure 1. Research location

the limited number of field observations; therefore, model performance was assessed using the validation subset. The validation points are explicitly reported to improve transparency and traceability of the model evaluation process. Multiple linear regression was applied to quantify the relationship between spectral reflectance variables and PM_{10} concentration. The model was evaluated using statistical metrics, including the correlation coefficient (R), coefficient of determination (R^2), and root mean square error (RMSE), based on both training and independent testing datasets.

Dataset

This study utilized two primary data sources, namely Landsat 8 OLI/TIRS Collection 2 Level-1 imagery and field-based PM_{10} measurements. The Landsat 8 imagery was acquired on 27 March 2025 from official United States Geological Survey (USGS) Earth Explorer platform (https://earthexplorer.usgs.gov/), with Scene ID LC81140642025086LGN00 and Product ID LC08_L1TP_114064_20250327_20250401_02_T1 (Path 114/Row 064). The dataset belongs to Collection 2 Tier 1 (T1), which provides high geometric accuracy suitable for quantitative environmental analysis. The Landsat 8 OLI/TIRS dataset consists of multispectral bands with a spatial resolution of 30 m, a panchromatic band with a spatial resolution of 15 m, and thermal bands resampled to 30 m. The spectral characteristics of each Landsat 8 band are presented in Table 1.

The selected image had a total cloud cover of 34.37% and land cloud cover of 39.18%, as recorded in the Landsat 8 metadata. This condition was considered as an image quality limitation. Image preprocessing was performed on raster-based Landsat 8 data and included AOI clipping, radiometric correction, TOA reflectance conversion, and DOS atmospheric correction. Therefore, point cloud filtering was not applied in the preprocessing

Table 1. Spectral characteristics of Landsat 8 OLI/TIRS imagery

Band	Band name	Wavelength (μm)	Spatial resolution (m)
1	Coastal/Aerosol	0.435–0.451	30
2	Blue	0.452–0.512	30
3	Green	0.533–0.590	30
4	Red	0.636–0.673	30
5	Near Infrared (NIR)	0.851–0.879	30
6	Shortwave Infrared 1 (SWIR 1)	1.566–1.651	30
7	Shortwave Infrared 2 (SWIR 2)	2.107–2.294	30
8	Panchromatic	0.503–0.676	15
9	Cirrus	1.363–1.384	30
10	Thermal Infrared 1 (TIRS 1)	10.60–11.19	100
11	Thermal Infrared 2 (TIRS 2)	11.50–12.51	100

workflow. Solar geometry parameters, including sun elevation and azimuth angles, were incorporated during reflectance normalization.

Image preprocessing included raster clipping based on the area of interest (AOI), radiometric correction, conversion of digital number (DN) values to top of atmosphere (TOA) reflectance, and atmospheric correction using the dark object subtraction (DOS) method. The AOI was defined using a shapefile (SHP) representing the administrative boundary of Makassar City to ensure spatial consistency between satellite imagery, field measurements, and PM_{10} modeling outputs. All spatial processing procedures, including raster clipping, radiometric correction, atmospheric correction, reflectance extraction, and PM_{10} raster mapping, were performed using ArcGIS 10.5. Statistical analyses, including correlation analysis and multiple linear regression, were conducted using IBM SPSS Statistics version 17.0. The correlation coefficient (R) and coefficient of determination (R^2) were obtained from the regression output, while Microsoft Excel was used for data tabulation and RMSE calculation. No additional programming libraries were used because the analysis was conducted using GUI-based software.

Spectral reflectance values from Landsat 8 Bands 1–4 were extracted using a point-based pixel extraction method. Each PM_{10} sampling point was overlaid on the corrected Landsat 8 raster, and the reflectance value was taken from the pixel spatially overlapping the field measurement point. Since Landsat 8 OLI multispectral bands have a 30 m spatial resolution, the extraction window corresponded to a single 30 × 30 m pixel.

Following preprocessing, spectral reflectance values were extracted from visible bands, specifically Band 1 (coastal aerosol), Band 2 (blue), Band 3 (green), and Band 4 (red), which are sensitive to atmospheric scattering and aerosol particles. Visible bands are widely applied in particulate estimation because aerosol interactions are stronger within visible wavelengths, resulting in significant relationships with PM_{10} concentration (Gupta and Christopher, 2009; Kumar et al., 2011). Reflectance values derived from these bands were subsequently integrated with field-based PM_{10} measurements to predict satellite-based PM_{10} concentration estimates (Figure 2).

The second dataset used in this study consisted of field-based PM_{10} measurements collected from 30 observation points distributed across various urban activity zones in Makassar. These measurements represented actual ambient air quality conditions and were used as the dependent variable for model calibration and validation of satellite-derived PM_{10} estimates. Field sampling was conducted in March 2025 using a high volume air sampler (HVAS) with the gravimetric method following SNI 7119.15:2016 for particulate matter ≤10 μm. PM_{10} particles were collected using fiberglass filter paper with a diameter of 11 cm and a pore size of 1.6 μm, enabling efficient capture of suspended particulate matter. Filters were weighed before and after sampling under controlled laboratory conditions to determine particulate mass accumulation. PM_{10} concentration was calculated from the difference in filter mass divided by the total sampled air volume. To improve methodological transparency and reproducibility, the calculation procedure used to derive PM_{10} concentration from field measurements

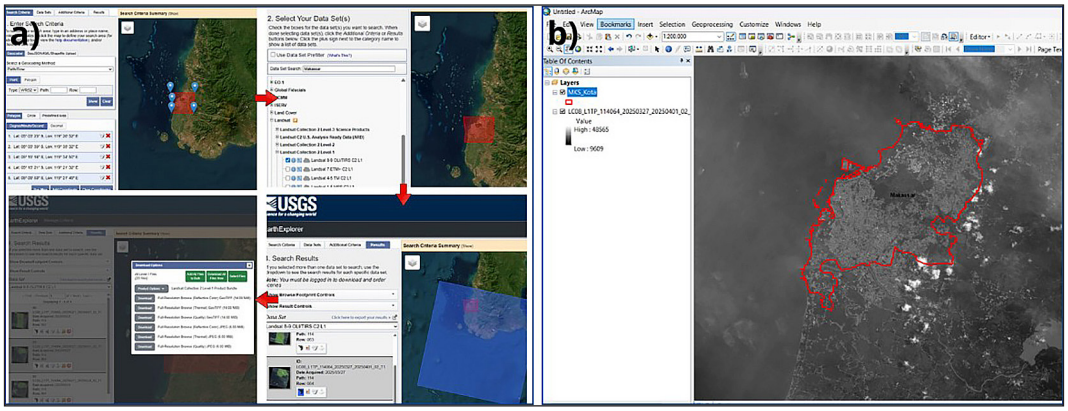

Figure 2. (a) Step-by-step workflow of Landsat 8 data acquisition using the USGS EarthExplorer platform; (b) delineation of the area of interest (AOI)

is illustrated in Figure 3. The flowchart summarizes the sequential steps applied in the gravimetric analysis, including airflow correction, standard air volume calculation, and determination of PM_{10} concentration based on filter mass differences and sampled air volume.

Sampling was performed at four daily intervals: morning, afternoon, evening, and night time, with each measurement lasting one hour. Approximate sampling times for each interval are presented in Table 2. Raw measurements from all intervals were recorded before averaging to obtain daily PM_{10} concentrations for each observation point, ensuring comparability with satellite acquisition time. Temporal comparability between satellite imagery and field measurements was addressed by using field-based PM_{10} data collected within the same observation period as the Landsat 8 acquisition. The field measurements were averaged into 24-hour PM_{10} concentrations to represent daily ambient conditions and reduce the influence of short-term fluctuations from traffic peaks, temporary local emissions, and hourly atmospheric variability.

Each sampling record included geographic coordinates, measurement time, filter identification, and field observations. The 30 sampling locations were distributed across 14 districts representing transportation corridors, industrial and port areas, residential zones, and vegetated environments to capture spatial variability in PM_{10} concentrations. The spatial distribution of sampling points is shown in Figure 4f, while detailed measurement information is provided in Table 2. Figure 3 presents the workflow used to calculate PM_{10} concentration from field sampling results.

Methods

The research workflow began with the preprocessing of Landsat 8 imagery, which included defining the AOI, raster clipping, and applying radiometric and atmospheric corrections to ensure the accuracy of spectral reflectance values. Subsequently, input variables were extracted from the imagery in the form of reflectance values for each spectral band and analyzed using multiple linear regression, with PM_{10} concentrations obtained from field measurements serving as the dependent variable. This analysis aimed to identify spectral bands that are sensitive to variations in near-surface particulate concentrations and to use them as the basis for developing a PM_{10} estimation model.

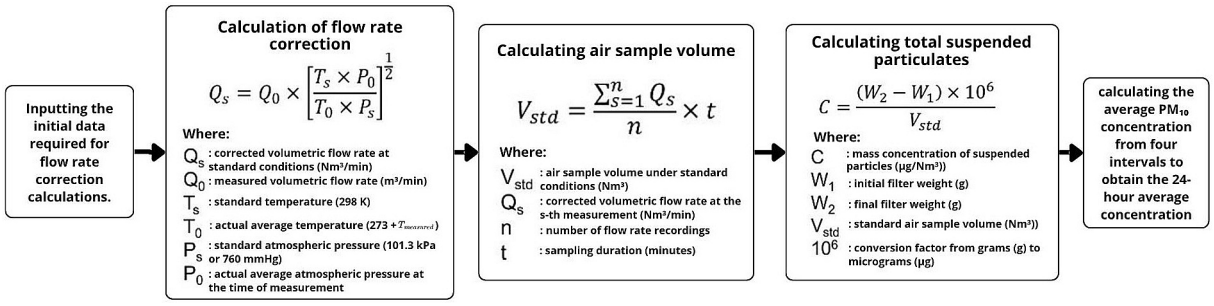

Figure 3. Flowchart of 24-hour average PM_{10} concentration calculation from field measurements

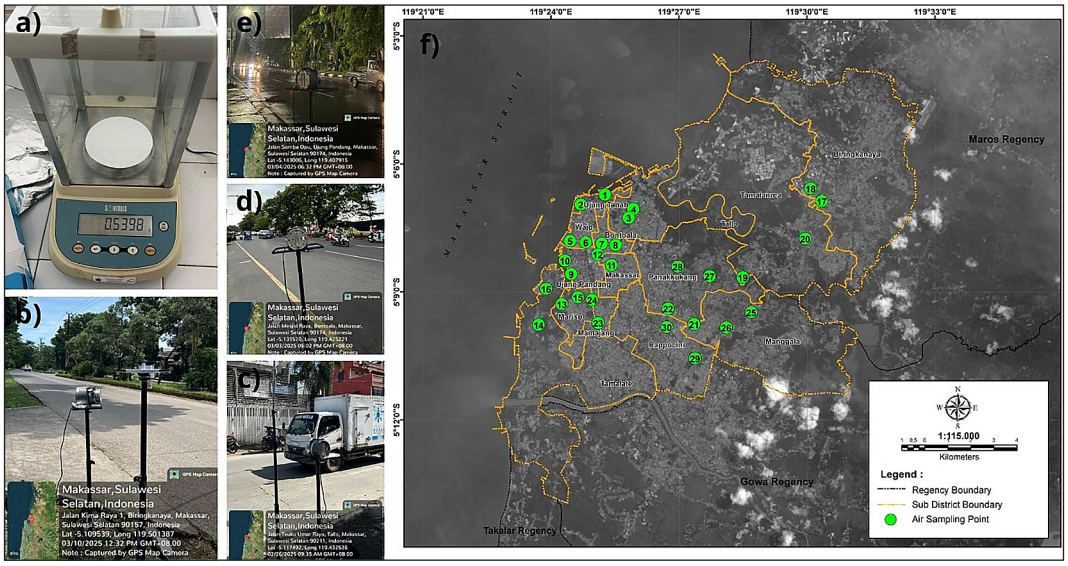

Figure 4. (a) Filter weighing stage; (b) Morning interval measurement using a HVAS; (c) Afternoon interval measurement using a HVAS; (d) Evening interval measurement using a HVAS; (e) Nighttime interval measurement using a HVAS: (f) Spatial distribution of sampling locations

The spectral bands utilized in this study include Band 1, Band 2, Band 3, and Band 4 (near-UV and visible bands) of Landsat 8 imagery, which are associated with the scattering of electromagnetic radiation by aerosol particles in the atmosphere. The estimated values obtained from the derived algorithmic equation were subsequently validated against field measurement data collected from the monitoring points to assess the level of agreement and identify potential discrepancies. Following the validation process, the data were analyzed spatially to produce a pollutant distribution map across the entire study area. The overall PM_{10} modeling workflow is summarized in Figure 5.

Pre-processing

Satellite image data correction

Satellite image preprocessing is a fundamental step in ensuring the accuracy and reliability of remote sensing data for environmental analysis, particularly for urban air quality monitoring. In this study, two main correction techniques were applied to Landsat 8 imagery: radiometric correction and atmospheric correction. Each correction method addresses specific sources of error and improves the spatial, spectral, and geometric fidelity of the satellite data, allowing the imagery to more accurately represent actual surface conditions. Radiometric correction aims to remove noise and inconsistencies in pixel intensity values caused by varying illumination conditions, sensor calibration errors, and atmospheric interference during image acquisition (Gopan et al., 2017). In this study, radiometric correction involved converting the raw DN values of satellite imagery into TOA reflectance to ensure the consistency of spectral brightness across different images and acquisition times. The initial step of this correction process was converting the raw DN values of each pixel into spectral radiance (Lλ) using calibration coefficients provided in the metadata file of the Landsat 8 imagery. The conversion equation is expressed as follows:

$$L\lambda = ML \times Qcal + AL \tag{1}$$

where: $L\lambda$ is the spectral radiance ($W \cdot m^{-2} \cdot sr^{-1} \cdot \mu m^{-1}$), ML denotes the radiance multiplicative scaling factor (radiance mult band); A_L represents the radiance additive scaling factor (radiance add band); and $Qcal$ is the calibrated pixel DN.

The next step is to convert the spectral radiance into TOA reflectance to ensure that spectral brightness values are consistent across different images and acquisition times. The conversion to TOA reflectance can be performed directly using reflectance coefficients provided in the metadata or by applying the standard formula recommended by the USGS as follows:

$$\rho\lambda = \frac{\pi L_\lambda d^2}{E_{sun,\lambda} cos\theta_s} \tag{2}$$

Table 2. Ambient air measurement points

Measurement point	Location (District)	Coordinate X (Longitude)	Coordinate Y (Latitude)	Interval (WITA)	W1 (g)	W2 (g)	Interval concentration (μg/m³)	24-hour average PM_{10} concentration (μg/m³)
SP 1	Ujung Tanah	119.42104	-5.112004	08.00–09.00	0.533	0.538	135.62	218.07
				12.00–13.00	0.530	0.537	184.66	
				15.30–16.30	0.529	0.544	321.38	
				19.00–20.00	0.513	0.522	230.60	
SP 2	Ujung Tanah	119.41161	-5.115785	09.00–10.00	0.518	0.523	141.93	202.62
				10.30–11.30	0.515	0.520	130.94	
				17.00–18.00	0.512	0.522	290.49	
				18.00–19.00	0.532	0.541	247.11	
SP 3	Tallo	119.43032	-5.121004	08.00–09.00	0.518	0.519	27.58	178.18
				12.00–13.00	0.523	0.528	151.23	
				15.30–16.30	0.517	0.526	265.97	
				19.00–20.00	0.518	0.526	267.95	
SP 4	Tallo	119.43216	-5.117567	09.00–10.00	0.515	0.523	240.50	243.63
				10.30–11.30	0.529	0.537	229.48	
				17.00–18.00	0.528	0.540	368.26	
				18.00–19.00	0.531	0.535	136.27	
SP 5	Wajo	119.40742	-5.13003	08.00–09.00	0.519	0.528	223.96	186.69
				12.00–13.00	0.523	0.529	162.28	
				15.30–16.30	0.519	0.526	175.66	
				19.00–20.00	0.539	0.546	184.84	
SP 6	Wajo	119.41357	-5.130593	09.00–10.00	0.515	0.521	145.27	108.03
				10.30–11.30	0.529	0.534	116.06	
				17.00–18.00	0.522	0.524	49.58	
				18.00–19.00	0.513	0.518	121.22	
SP 7	Bontoala	119.41982	-5.131092	08.00–09.00	0.531	0.537	141.80	149.16
				12.00–13.00	0.515	0.520	124.64	
				15.30–16.30	0.515	0.527	295.81	
				19.00–20.00	0.518	0.520	34.41	
SP 8	Bontoala	119.42522	-5.131589	09.00–10.00	0.521	0.526	277.81	178.76
				10.30–11.30	0.519	0.524	126.80	
				17.00–18.00	0.537	0.545	161.05	
				18.00–19.00	0.518	0.522	149.39	
SP 9	Ujung Pandang	119.40786	-5.143001	08.00–09.00	0.527	0.530	68.53	182.94
				12.00–13.00	0.517	0.524	177.24	
				15.30–16.30	0.531	0.542	262.54	
				19.00–20.00	0.514	0.523	223.45	
SP 10	Ujung Pandang	119.40545	-5.137727	09.00–10.00	0.528	0.531	61.23	216.29
				10.30–11.30	0.521	0.528	186.68	
				17.00–18.00	0.508	0.520	302.32	
				18.00–19.00	0.507	0.519	314.94	
SP 11	Makassar	119.42359	-5.139478	08.00–09.00	0.522	0.525	59.11	199.41
				12.00–13.00	0.510	0.515	131.16	
				15.30–16.30	0.510	0.525	331.27	
				19.00–20.00	0.507	0.520	276.08	

Measurement point	Location (District)	Coordinate X (Longitude)	Coordinate Y (Latitude)	Interval (WITA)	W1 (g)	W2 (g)	Interval concentration (μg/m³)	24-hour average PM_{10} concentration (μg/m³)
SP 12	Makassar	119.41826	-5.135358	09.00–10.00	0.528	0.535	170.30	157.36
				10.30–11.30	0.515	0.521	127.00	
				17.00–18.00	0.521	0.530	219.31	
				18.00–19.00	0.516	0.520	112.82	
SP 13	Mariso	119.40418	-5.154752	08.00–09.00	0.537	0.549	299.91	226.05
				12.00–13.00	0.540	0.545	105.29	
				15.30–16.30	0.520	0.535	366.81	
				19.00–20.00	0.522	0.527	132.21	
SP 14	Tamalate	119.39514	-5.162849	09.00–10.00	0.520	0.531	280.47	199.18
				10.30–11.30	0.517	0.525	188.63	
				17.00–18.00	0.530	0.538	214.88	
				18.00–19.00	0.532	0.537	112.76	
SP 15	Mariso	119.41051	-5.152054	08.00–09.00	0.532	0.534	54.32	130.34
				12.00–13.00	0.527	0.532	101.69	
				15.30–16.30	0.527	0.531	99.56	
				19.00–20.00	0.517	0.528	265.77	
SP 16	Tamalate	119.39806	-5.148736	09.00–10.00	0.523	0.536	316.78	167.16
				10.30–11.30	0.521	0.531	232.95	
				17.00–18.00	0.535	0.539	87.08	
				18.00–19.00	0.517	0.518	31.84	
SP 17	Biringkanaya	119.50577	-5.114465	08.00–09.00	0.514	0.517	71.63	262.94
				12.00–13.00	0.516	0.531	349.04	
				15.30–16.30	0.527	0.532	270.33	
				19.00–20.00	0.512	0.527	360.76	
SP 18	Biringkanaya	119.50143	-5.109536	09.00–10.00	0.519	0.528	220.64	199.49
				10.30–11.30	0.519	0.525	145.52	
				17.00–18.00	0.514	0.530	388.08	
				18.00–19.00	0.540	0.542	43.74	
SP 19	Tamalanrea	119.47488	-5.144292	08.00–09.00	0.512	0.522	251.79	257.99
				12.00–13.00	0.523	0.534	277.26	
				15.30–16.30	0.509	0.523	344.14	
				19.00–20.00	0.529	0.535	158.78	
SP 20	Tamalanrea	119.49931	-5.129157	09.00–10.00	0.517	0.523	150.05	192.21
				10.30–11.30	0.524	0.530	152.83	
				17.00–18.00	0.515	0.524	223.44	
				18.00–19.00	0.518	0.528	242.51	
SP 21	Manggala	119.4559	-5.162571	08.00–09.00	0.515	0.527	293.72	235.01
				12.00–13.00	0.513	0.525	281.38	
				15.30–16.30	0.528	0.540	313.60	
				19.00–20.00	0.509	0.512	51.34	
SP 22	Panakkukang	119.44571	-5.156465	09.00–10.00	0.522	0.523	27.16	234.50
				10.30–11.30	0.503	0.512	230.16	
				17.00–18.00	0.520	0.535	364.39	
				18.00–19.00	0.504	0.517	316.29	

Measurement point	Location (District)	Coordinate X (Longitude)	Coordinate Y (Latitude)	Interval (WITA)	W1 (g)	W2 (g)	Interval concentration (μg/m³)	24-hour average PM_{10} concentration (μg/m³)
SP 23	Mamajang	119.41845	-5.162069	08.00–09.00	0.514	0.531	418.48	191.67
				12.00–13.00	0.512	0.517	118.59	
				15.30–16.30	0.529	0.533	84.19	
				19.00–20.00	0.514	0.520	145.41	
SP 24	Mamajang	119.41608	-5.153083	09.00–10.00	0.521	0.523	71.37	102.24
				10.30–11.30	0.524	0.530	164.45	
				17.00–18.00	0.514	0.516	52.40	
				18.00–19.00	0.521	0.526	120.74	
SP 25	Manggala	119.47823	-5.157948	08.00–09.00	0.528	0.541	296.81	211.00
				12.00–13.00	0.514	0.521	152.94	
				15.30–16.30	0.515	0.516	37.06	
				19.00–20.00	0.526	0.541	357.20	
SP 26	Manggala	119.46845	-5.1639	09.00–10.00	0.531	0.535	88.85	214.62
				10.30–11.30	0.524	0.533	206.58	
				17.00–18.00	0.524	0.535	283.62	
				18.00–19.00	0.530	0.542	279.44	
SP 27	Panakkukang	119.4619	-5.143785	08.00–09.00	0.515	0.516	42.42	184.19
				12.00–13.00	0.515	0.521	176.00	
				15.30–16.30	0.526	0.541	414.33	
				19.00–20.00	0.511	0.515	104.02	
SP 28	Panakkukang	119.44949	-5.140062	09.00–10.00	0.528	0.535	169.30	251.97
				10.30–11.30	0.510	0.521	274.64	
				17.00–18.00	0.528	0.542	335.38	
				18.00–19.00	0.512	0.521	228.57	
SP 29	Rappocini	119.45626	-5.175949	08.00–09.00	0.527	0.535	202.52	185.43
				12.00–13.00	0.517	0.523	145.69	
				15.30–16.30	0.531	0.545	345.00	
				19.00–20.00	0.517	0.519	48.51	
SP 30	Rappocini	119.44523	-5.163729	09.00–10.00	0.527	0.538	257.23	148.62
				10.30–11.30	0.520	0.530	237.06	
				17.00–18.00	0.517	0.519	51.69	
				18.00–19.00	0.529	0.531	48.51	

where: $\rho\lambda$ is the dimensionless TOA reflectance, d is the Earth–Sun distance in astronomical units (AU) on the acquisition date, $Esun,\lambda$ is the mean solar exo-atmospheric irradiance at wavelength λ, and θs is the solar zenith angle (90° − solar elevation angle).

If reflectance scaling factors provided in the metadata are used, the TOA conversion can be expressed in a simpler form as:

$$\rho\lambda = \frac{M_\rho \times Q_{cal} + A_\rho}{cos\theta_s} \quad (3)$$

where: $M\rho$ and $A\rho$ are the reflectance multiplicative and additive scaling factors for each band, respectively.

Through this process, the reflectance value of each pixel has been normalized, making it suitable for subsequent spectral analyses such as vegetation indices, land surface temperature estimation, and pollutant detection.

Atmospheric correction removes the effects of atmospheric scattering and absorption from surface reflectance measurements. It is an essential pre-processing step to eliminate atmospheric scattering and absorption effects that may distort the surface reflectance values derived from satellite imagery. One commonly used technique is the DOS method, which operates under the assumption that certain features

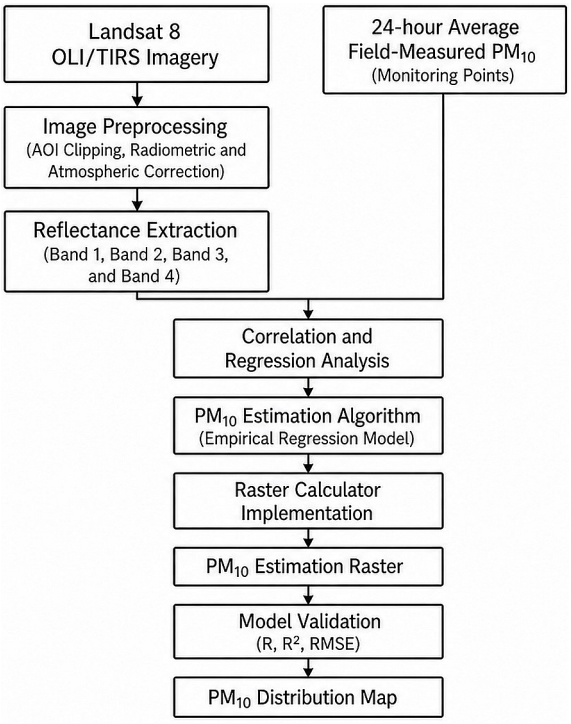

Figure 5. Research methodology

on the Earth's surface, such as deep water bodies, dense shadows, or asphalt, have near-zero reflectance in specific spectral bands (Ding et al., 2015). In this approach, dark objects are used as references to estimate the atmospheric scattering contribution recorded by the satellite sensor. The correction is performed by subtracting the minimum digital value in each spectral band from the measured radiance values in the imagery. In this study, dark objects for the DOS correction were selected from low-reflectance pixels representing deep water bodies within the Landsat 8 scene. These pixels were assumed to have near-zero reflectance in the visible bands. The minimum value in each band was then used as the dark-object reference to reduce atmospheric scattering effects. Mathematically, the atmospheric correction process using the DOS method can be expressed as follows:

$$L_{corrected} = L_{measured} - L_{min} \quad (4)$$

where: $L_{corrected}$ is the radiance value of the image after atmospheric correction, $L_{measured}$ is the radiance value or digital number (DN) recorded by the satellite sensor before correction, and L_{min} is the minimum radiance value assumed to originate from dark objects in each spectral band.

By subtracting this minimum radiance value from the measured radiance, the contribution of atmospheric scattering can be minimized, resulting in reflectance values that are more representative of actual surface conditions. This correction process is essential to improve the accuracy of spectral analysis, particularly in studies that utilize satellite imagery to estimate environmental parameters such as PM_{10} particulate concentration.

Processing

Following AOI clipping and radiometric correction, Landsat 8 DN values were converted into TOA reflectance using metadata parameters. Atmospheric correction was then applied using the DOS method. The DOS-corrected reflectance was used as an approximation of surface reflectance and served as the predictor variable in the PM_{10} regression models, rather than raw DN values or uncorrected TOA reflectance. These corrected reflectance values were then analyzed using multiple linear regression to derive a PM_{10} predictive equation. The resulting equation is then implemented in the Raster Calculator within ArcGIS 10.5 to model the spatial distribution of PM_{10} concentration. The PM_{10} distribution map is presented based on the modeling results with the highest coefficient of determination (R^2) and the lowest root mean square error (RMSE). The final output is an image of PM_{10} concentration distribution, visualized using a color scheme corresponding to concentration classes.

Aerosol optical thickness and PM_{10} correlation

The relationship between aerosol optical thickness (AOT) and atmospheric reflectance can be expressed as follows (Othman et al., 2010):

$$\tau_a = \left(\frac{4\mu\mu_o}{\omega_o P_a(\theta_{s'}\theta_{v'}\phi)}\right)\rho_{atm}(\theta_{s'}\theta_{v'}\phi) \quad (5)$$

where: τa represents aerosol optical thickness, ρatm represents atmospheric reflectance, ω_o is the single scattering albedo, Pa (θ_s, θ_v, ϕ) is the aerosol scattering phase function, μ is the cosine of the sensor viewing direction, and μ_o is the cosine of the incident solar radiation direction.

The geometric and aerosol scattering parameters can be simplified into an empirical coefficient (a_j). Therefore, the relationship between AOT and atmospheric reflectance can be written as:

$$\tau_{a_{(\lambda)}} = a_j \rho_{atm(\lambda i)} \quad (6)$$

Based on this linear relationship, the AOT–reflectance formulation was used as a conceptual basis for developing an empirical PM_{10} regression model using Landsat 8 spectral bands. For multi-band Landsat 8 data, the AOT model can be expressed as:

$$\mathrm{AOT}(\lambda) = a_0 + a_1 R_{\lambda 1} + a_2 R_{\lambda 2} + a_3 R_{\lambda 3} + a_4 R_{\lambda 4} \quad (7)$$

where: $R\lambda i$ represents the atmospheric reflectance of Landsat 8 spectral bands (i = 1, 2, 3, 4), while aj represents the empirical coefficient associated with each spectral band.

The application of this formulation to the PM_{10} regression model is further described in the model development section.

Correlation analysis was conducted to support the use of Landsat 8 spectral bands as predictor variables for PM_{10} estimation. As shown in Table 3, PM_{10} showed strong and statistically significant positive correlations with Band 1, Band 2, Band 3, and Band 4, with correlation coefficients ranging from 0.709 to 0.755 ($p < 0.01$). These findings indicate that the selected spectral bands are responsive to variations in PM_{10} concentration and can be considered suitable for subsequent empirical regression modeling.

However, high inter-band correlations were also observed ($r > 0.97$), indicating multicollinearity among the spectral bands. This condition is common in multispectral remote sensing data because adjacent visible bands often have overlapping spectral responses. Therefore, multicollinearity was handled through inter-band correlation analysis and by limiting the interpretation of the regression coefficients. Individual band coefficients were not interpreted as separate physical effects of each spectral band. Instead, the regression models were treated as empirical predictive models, and model selection was based on their agreement with field measurements.

PM_{10} regression model development and validation

Based on the correlation analysis presented in the previous section, Landsat 8 Band 1, Band 2, Band 3, and Band 4 showed strong and statistically significant positive relationships with PM_{10} concentration in Makassar City, with correlation coefficients ranging from 0.709 to 0.755 ($p < 0.01$). These results provide the basis for using the selected bands as predictor variables in the development of an empirical regression model. Referring to Equation 7, the multi-band AOT formulation was adapted into an empirical regression model to estimate PM_{10} concentration as follows:

$$PM_{10} = a_0 + a_1 R_{\lambda 1} + a_2 R_{\lambda 2} + a_3 R_{\lambda 3} + a_4 R_{\lambda 4} \quad (8)$$

where: PM_{10} represents the estimated particulate matter concentration, while $R_{\lambda 1}$, $R_{\lambda 2}$, $R_{\lambda 3}$, and $R_{\lambda 4}$ represent the atmospheric reflectance values of Landsat 8 Band 1, Band 2, Band 3, and Band 4, respectively. The coefficient a_0 represents the regression intercept, while a_1, a_2, a_3, and a_4 represent regression coefficients derived from multiple linear regression analysis.

Several band combinations were explored to generate alternative algorithms for PM_{10} estimation. The notations B1, B2, B3, and B4 in the regression equations represent the atmospheric reflectance values of the corresponding Landsat 8 bands. The regression equations for each band combination are presented in Table 4, while the statistical performance of each model, including the correlation coefficient and coefficient of determination, is presented in the Results section.

Table 4 shows that each band combination produced a different regression algorithm for PM_{10} estimation in Makassar City. All algorithms were applied separately to the Landsat 8 imagery using raster calculator to generate PM_{10} estimation rasters for each model.

The estimation results from each model were then validated using field measurement data.

Table 3. Correlation between PM_{10} and Landsat 8 spectral bands

Variable pair	Correlation coefficient (r)	p-value	Interpretation
PM_{10} – Band 1	0.722	0.002	Strong positive correlation
PM_{10} – Band 2	0.732	0.002	Strong positive correlation
PM_{10} – Band 3	0.755	0.001	Strong positive correlation
PM_{10} – Band 4	0.709	0.003	Strong positive correlation

Table 4. Regression algorithms for PM_{10} estimation using Landsat 8 spectral bands

Model	Band combination	Regression algorithm
A	B1, B3, B4	PM_{10} = -29.939 + 435.524(B1) + 2124.475(B3) - 1175.342(B4)
B	B1, B2, B3, B4	PM_{10} = 181.051 - 6618.074(B1) + 6930.677(B2) + 2210.701(B3) - 1711.152(B4)
C	B2, B3, B4	PM_{10} = -60.201 + 978.020(B2) + 2384.398(B3) - 1835.955(B4)

Model RMSE. Field-based validation is required to assess the reliability of remote sensing-based models (Loew et al., 2017), while RMSE was used to quantify the deviation between predicted and observed values (Chai and Draxler, 2014). RMSE was calculated using the following equation:

$$RMSE = \sqrt{\frac{1}{n}\sum_{i=1}^{n}(yi - \hat{y}i)^2} \qquad (9)$$

where: yi represents the field-measured PM_{10} concentration at the i-th point, $\hat{y}i$ represents the estimated PM_{10} concentration from the model at the same point, and n is the number of validation points.

The model with the lowest RMSE was selected as the model with the best estimation performance.

Because high inter-band correlations were identified, model evaluation was focused on predictive performance against field measurement data. Therefore, the best-performing model was determined based on the correlation coefficient, coefficient of determination, and primarily the RMSE value, and was subsequently used as an empirical model for spatial PM_{10} estimation in Makassar City.

RESULTS

PM_{10} concentration modeling

The PM_{10} concentration models were developed using multiple linear regression based on corrected Landsat 8 reflectance values and 24-hour average field-measured PM_{10} concentrations. Landsat 8 Band 1, Band 2, Band 3, and Band 4 were used as predictor variables, while field-measured PM_{10} concentration was used as the dependent variable. Three regression models were evaluated based on different band combinations, as described in the methodology section.

Table 5 presents the statistical performance and estimated PM_{10} concentration range of each regression model. The correlation coefficient (R) ranged from 0.775 to 0.811, while the coefficient of determination (R^2) ranged from 0.601 to 0.658. The significance values of all models were below 0.05, indicating that the overall regression models showed statistically significant relationships with field-measured PM_{10} concentrations. The estimated PM_{10} ranges represent pixel-based raster values generated from each regression algorithm across Makassar City.

The results indicate that all regression models produced strong relationships between Landsat 8 reflectance values and field-measured PM_{10} concentrations. Differences in R, R^2, significance values, and estimated concentration ranges show that each band combination generated different model responses. The regression equations used to generate these raster outputs have been described in the methodology section.

To demonstrate the raster-based implementation of the model, the PM_{10} estimation algorithm was applied to the corrected Landsat 8 reflectance rasters using the ArcGIS Raster Calculator. The input layers consisted of corrected reflectance rasters from Band 1, Band 2, Band 3, and Band 4. Figure 6 is presented as processing evidence showing how the PM_{10} estimation algorithm was implemented in the ArcGIS Raster Calculator.

After the regression algorithms were applied, PM_{10} estimation raster outputs were generated for

Table 5. Statistical summary and estimated pm_{10} range of regression models

Model	Band combination	R	R^2	Sig.	Estimated PM_{10} range (μg/m³)
Model A	B1, B3, B4	0.775	0.601	0.015	108.56–861.82
Model B	B1, B2, B3, B4	0.811	0.658	0.020	57.779–976.77
Model C	B2, B3, B4	0.784	0.615	0.019	62.64–896.42

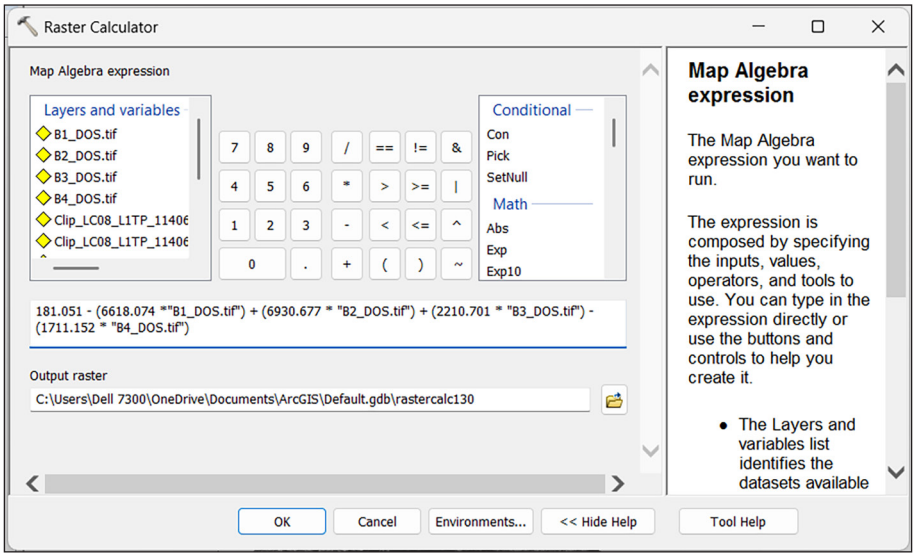

Figure 6. PM_{10} algorithm implementation in ArcGIS (10.5) raster calculator

each model. The raster maps from the three models are presented in Figure 7 as spatial estimation outputs for Makassar City.

PM_{10} model accuracy results

Model validation was conducted to evaluate the agreement between satellite-based PM10 estimates and field-measured PM10 concentrations. The validation process used six independent testing points that were not included in the model development stage. The estimated PM10 values generated from Model A, Model B, and Model C were compared with field-measured PM10 concentrations using the correlation coefficient (R), coefficient of determination (R^2), and RMSE.

Table 6 summarizes the validation results of the three PM10 estimation models using six independent validation points. The validation R values ranged from 0.673 to 0.781, while the R^2 values ranged from 0.453 to 0.609. The total squared error values are included to explicitly show the basis of the RMSE calculation. The RMSE values ranged from 33.1083 to 33.8462 µg/m³, indicating different levels of prediction error among the regression models. The RMSE values were calculated from the squared differences between field-measured PM10 concentrations and model-estimated PM10 values. The inclusion of the total squared error values provides transparency in the calculation process and supports the reproducibility of the validation results.

The scatter plots between field-measured PM10 and estimated PM10 concentrations for each regression model are presented in Figure 8. These plots provide visual evidence of the validation process and show the relationship between observed and estimated values at the validation points. The coefficient of determination values shown in Figure 8 were 0.583 for Model A, 0.609 for Model B,

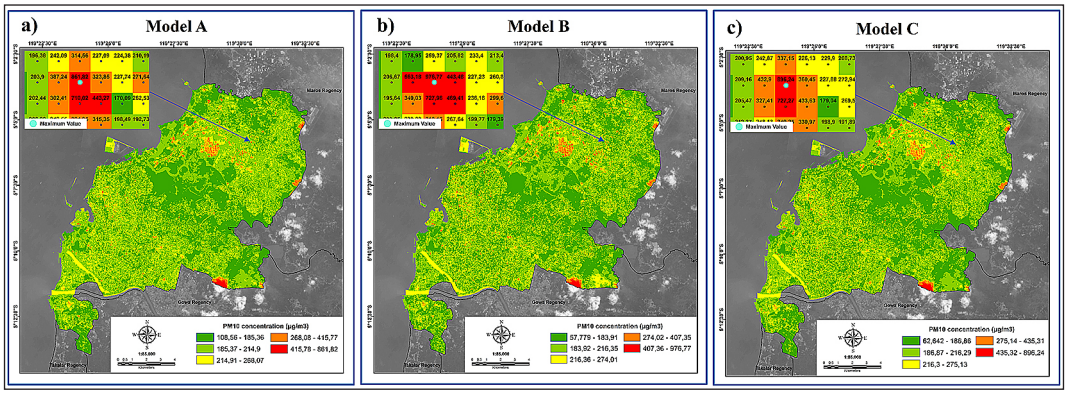

Figure 7. Estimated PM_{10} concentration maps of Makassar City generated from Model A, Model B, and Model C

Table 6. Validation summary of PM10 estimation models

Model	n	R	R^2	$\Sigma(yi - \hat{y}i)^2$	RMSE (μg/m³)
Model A	6	0.764	0.583	6602.66	33.1729
Model B	6	0.781	0.609	6576.95	33.1083
Model C	6	0.673	0.453	6873.38	33.8462

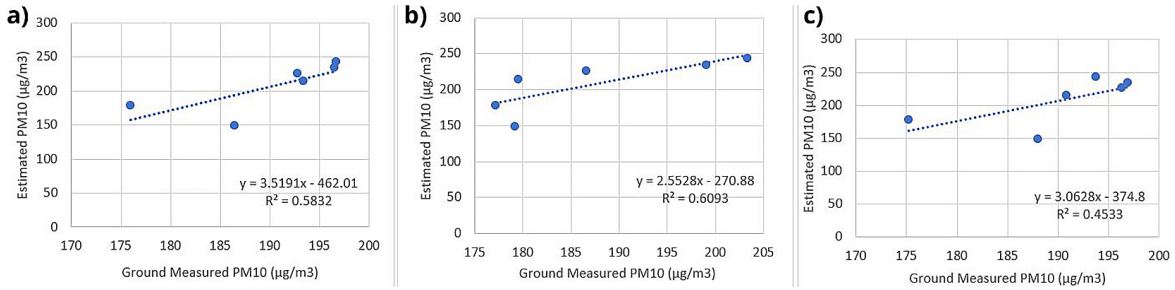

Figure 8. Scatter plots of field-measured and estimated PM10 concentrations for validation points: (a) Model A, (b) Model B, and (c) Model C

and 0.453 for Model C. These values indicate that the estimated PM10 concentrations from each model had different levels of correspondence with the field measurements.

Overall, the validation results demonstrate that the regression models were able to represent the variation pattern of PM10 concentrations to different extents. Differences between estimated and observed values remain at several validation points, reflecting the presence of prediction uncertainty in the satellite-based empirical models. Further interpretation of these differences is discussed in the Discussion section.

DISCUSSION

PM_{10} estimation model performance

The results indicate that PM_{10} estimation in Makassar was not determined solely by the general sensitivity of visible bands to aerosol scattering, but also by the ability of combined spectral bands to separate atmospheric signals from complex urban surface reflectance. Among the three models, Model B showed the highest statistical performance, with $R = 0.811$ and $R^2 = 0.658$ during model development. It also remained the most consistent model during validation, with $R = 0.781$, $R^2 = 0.609$, and the lowest RMSE of 33.1083 μg/m³. Although the differences in performance among the models were relatively small, the inclusion of Band 2 alongside Bands 1, 3, and 4 appears to provide a more stable empirical response for PM_{10} estimation compared with the more limited band combinations used in Models A and C.

The relevance of Model B lies not only in its statistical performance but also in its ability to represent the environmental complexity of Makassar. Band 1, as the coastal/aerosol band, enhances sensitivity to particle scattering at shorter wavelengths, while Bands 2–4 provide complementary information across the visible spectrum. This combination helps reduce ambiguity between aerosol-related signals and surface reflectance from buildings, roads, vegetation, and water bodies, which is a major challenge in urban remote sensing applications (Bilal and Qiu, 2018). Similar findings have shown that multispectral Landsat data can support PM_{10} estimation when calibrated with field measurements (Saraswat et al., 2017; Zhang et al., 2019; Heriza et al., 2023), and the importance of combining multiple spectral bands has also been emphasized in previous studies (Lin et al., 2021).

The spatial output further supports this interpretation. As shown in Figure 9, Model B produced a heterogeneous PM_{10} distribution pattern, with higher estimated concentrations mainly observed in the northern, central, and eastern parts of Makassar, particularly around Ujung Tanah, Tallo, Biringkanaya, Tamalanrea, Panakkukang, and Manggala. These areas are associated with port activities, dense transportation corridors, industrial zones, and rapidly developing urban settlements. The estimated range of Model B, approximately 57.78–976.77 μg/m³, should be interpreted with caution. The upper values exceed

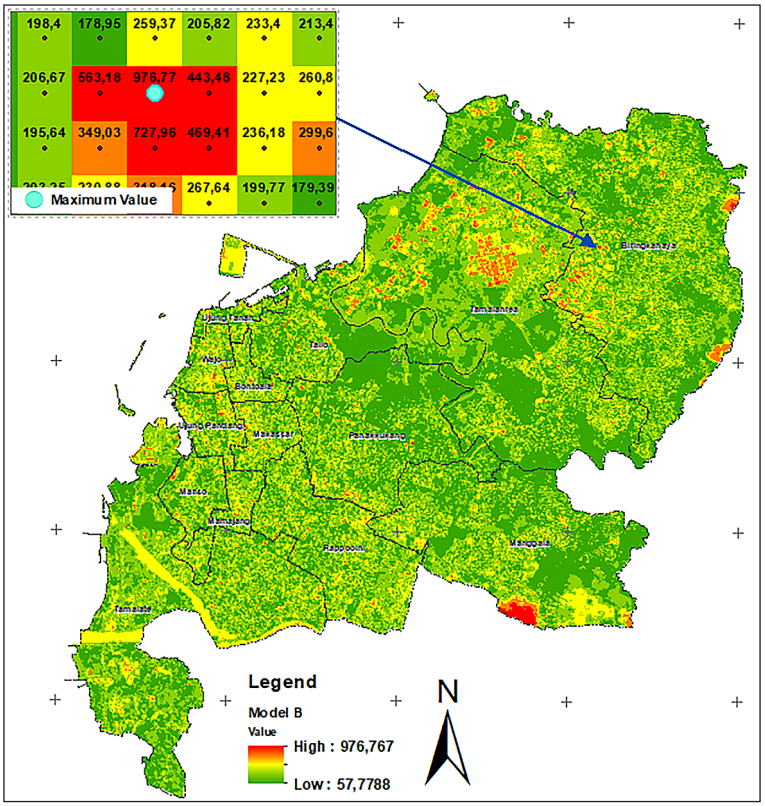

Figure 9. Spatial distribution of satellite-based PM_{10} estimation from Model B in Makassar City

typical ambient observations and likely reflect overestimation caused by extrapolation of the linear regression model when applied to pixel-level spectral variability beyond the conditions represented in the calibration dataset. Therefore, the model is more reliable for representing relative spatial patterns rather than absolute PM_{10} concentrations. Nevertheless, the wide range indicates that Model B is capable of capturing spatial heterogeneity across the study area.

Thus, the main implication of this study is that PM_{10} mapping in a tropical coastal city cannot rely solely on a simple visible band–aerosol relationship. Instead, a multi-band empirical approach is required to account for aerosol scattering, heterogeneous urban surfaces, and coastal environmental influences. In this context, the study contributes by demonstrating the applicability of Landsat 8 multispectral data for PM_{10} estimation in a tropical coastal urban environment, which remains relatively underrepresented in the literature.

Model accuracy and limitations in PM_{10} estimation

Although Model B produced the best validation performance, the RMSE value of 33.1083 $\mu g/m^3$ indicates moderate prediction accuracy and highlights the presence of uncertainty in satellite-based PM_{10} estimation. This level of error is consistent with previous studies using medium-resolution satellite imagery, where indirect estimation of particulate matter is affected by atmospheric complexity and interference from surface reflectance (Guang et al., 2016).

The detailed comparison between satellite-based estimated PM_{10} and ground-measured PM_{10} for Model B is presented in Table 7. The results show that Model B generally followed the variation of field-measured PM_{10}, although deviations remained at several validation points. The closest agreement was observed at SP 3, while larger differences occurred at SP 4, SP 13, SP 22, and SP 26. Figure 10 further illustrates that differences between estimated and measured PM_{10} were not uniform, indicating that spectral variables were sufficient to represent general spatial patterns but were less effective in capturing localized variability caused by short-term emissions, land-cover heterogeneity, and dynamic atmospheric conditions.

An important limitation of this study is the relatively small number of field observations, particularly in the validation dataset (n = 6). This constraint is common in field-based air quality

Table 7. Comparison of Ground-Measured and satellite-based estimated PM_{10} concentrations for Model B

Sample point	B1	B2	B3	B4	Satellite-based PM_{10} estimation (μg/m³)	Ground-based PM_{10} measurement (μg/m³)
SP 3	0.164	0.143	0.123	0.108	177.135	178.18
SP 4	0.184	0.167	0.148	0.143	203.368	243.63
SP 7	0.173	0.152	0.129	0.113	179.216	149.16
SP 13	0.173	0.151	0.130	0.110	186.566	226.05
SP 22	0.184	0.166	0.143	0.134	199.026	234.50
SP 26	0.187	0.167	0.143	0.138	179.493	214.62

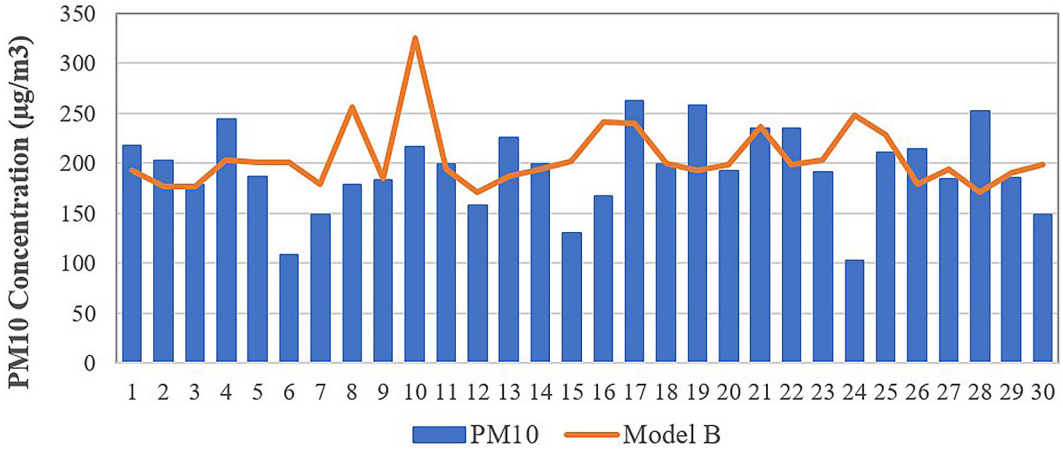

Figure 10. Comparison of PM_{10} concentrations obtained from ground-based measurements and those estimated using Model B

studies due to the logistical complexity and cost of high-volume air sampling. While the consistency between model development and validation results suggests that the model captures a meaningful empirical relationship, the limited sample size reduces statistical robustness, and the results should therefore be interpreted with caution. Future studies incorporating larger datasets and repeated validation are necessary to confirm the generalizability of the model.

Another important source of uncertainty is the temporal mismatch between satellite acquisition time and field measurements. In this study, 24-hour average PM_{10} concentrations were used to reduce short-term variability and better represent daily exposure conditions. Although this approach may reduce direct comparability with instantaneous satellite observations, it helps minimize the influence of transient emission spikes and provides a more stable basis for spatial analysis.

The presence of high inter-band correlations ($r > 0.97$) also indicates multicollinearity among predictor variables. While this condition may affect the stability and interpretability of regression coefficients, the primary objective of this study is predictive spatial mapping rather than parameter interpretation. Therefore, Model B should be interpreted as an empirical spatial prediction model, and its performance should be evaluated based on its agreement with field measurements rather than on the separate contribution of each spectral band.

Additional uncertainty may arise from Makassar's coastal setting, where sea-breeze circulation, aerosol mixing, and humidity can influence atmospheric optical properties. These factors, together with the indirect nature of satellite-based particulate estimation, contribute to discrepancies between estimated and observed values. These findings support previous recommendations to integrate meteorological variables, increase the number of observation points, and utilize higher-resolution imagery to improve PM_{10} estimation accuracy (Zaman et al., 2017; Irawadi and Razif, 2023; Putri and Bioresita, 2024). In a comparable regional context, Salsabila et al. (2026) also emphasized the importance of field validation and high-resolution spatial data for improving satellite-based air pollution estimation in South Sulawesi.

Implications for air quality monitoring

Overall, this study demonstrates that while satellite-based PM_{10} estimation using Landsat 8 is subject to uncertainty, it provides valuable insight into the spatial distribution of air pollution in data-scarce urban environments. The model should therefore be interpreted as a complementary tool for spatial analysis rather than a replacement for ground-based monitoring systems.

The integration of satellite imagery and field measurements offers practical value for supporting urban air quality management, particularly in regions where monitoring infrastructure is limited. By enabling broader spatial coverage, remote sensing approaches can help identify potential high-risk areas and support evidence-based environmental planning. In the case of Makassar, the results highlight the potential of multispectral satellite data to contribute to spatial air quality assessment in complex tropical coastal urban environments.

CONCLUSIONS

This study demonstrates that satellite-based PM_{10} estimation using Landsat 8 is feasible in a tropical coastal urban environment, but its primary value lies in its ability to capture spatial variability rather than to provide precise absolute concentrations. The results confirm that multispectral reflectance data can serve as a proxy for particulate matter distribution, particularly in data-scarce regions where ground-based monitoring is limited.

The findings consistently support the proposed hypotheses. First, Landsat 8 Bands 1–4 exhibited statistically significant relationships with field-measured PM_{10}, confirming their sensitivity to aerosol-related atmospheric signals. Second, the multi-band configuration (Model B) produced the most consistent performance across both model development and validation stages with $R = 0.811$ and $R^2 = 0.658$ during model development, and $R = 0.781$, $R^2 = 0.609$, and RMSE = 33.1083 $\mu g/m^3$ during validation, indicating that combining spectral information improves the robustness of empirical PM_{10} estimation. Third, while aerosol-sensitive bands play a critical role, their effectiveness is maximized when integrated with other visible bands, highlighting the importance of multi-band approaches in complex urban environments.

Beyond model comparison, the study provides an important contextual insight: PM_{10} estimation in tropical coastal cities cannot rely solely on simplified aerosol–reflectance relationships. Instead, it requires an empirical framework that accounts for the interaction between atmospheric scattering, heterogeneous urban surfaces, and coastal environmental dynamics. In this context, the combination of Band 1 with Bands 2–4 represents a practical and transferable spectral configuration for similar environments.

Importantly, the study does not propose a new algorithm but contributes by extending the applicability of Landsat-based PM_{10} modeling to medium-sized tropical coastal cities, which remain underrepresented in the literature. The results highlight that even moderate-accuracy models can provide meaningful spatial insights for environmental assessment and urban air quality management.

However, the findings should be interpreted in light of several limitations, including the relatively small number of field observations, the temporal mismatch between satellite acquisition and ground measurements, and the inherent limitations of linear regression applied to multispectral data. These factors introduce uncertainty and limit the use of the model for precise concentration estimation.

Overall, this study supports the use of satellite remote sensing as a complementary tool for air quality monitoring, particularly for identifying spatial patterns and potential high-risk areas.

REFERENCES

1. Bernardino, A. D., Palusci, O., Pini, A., Leuzzi, G., Cacciani, M., Pelliccioni, A., Monti, P. (2021). *Air circulation in urban areas.* Urban Microclimate Modelling for Comfort and Energy Studies, 195–221. https://doi.org/10.1007/978-3-030-65421-4_10
2. Bilal, M., Qiu, Z. (2018). Aerosol retrievals over bright urban surfaces using Landsat 8 images. *IGARSS 2018 - 2018 IEEE International Geoscience and Remote Sensing Symposium,* 7560–7563. https://doi.org/10.1109/IGARSS.2018.8517427
3. Chai, T., Draxler, R. R. (2014). Root mean square error (RMSE) or mean absolute error (MAE)? Arguments against avoiding RMSE in the literature. *Geoscientific Model Development, 7*(3), 1247–1250. https://doi.org/10.5194/gmd-7-1247-2014
4. Ding, H., Shi, J., Wang, Y., Wei, L. (2015). An improved dark-object subtraction technique for atmospheric correction of Landsat 8. *Proceedings, 9815*, 128–135. https://doi.org/10.1117/12.2205567
5. Fernández-Pacheco, V. M., López-Sánchez, C. A., Álvarez-Álvarez, E., López, M. J. S.,

García-Expósito, L., Yudego, E. A., Carús-Candás, J. L. (2018). Estimation of PM10 distribution using Landsat5 and Landsat8 remote sensing. *Proceedings 2*(23), 1430. https://doi.org/10.3390/PROCEEDINGS2231430

6. Gopan, L., Venkateswarlu, E., Nair, T., P.Swamy, G., Krishna, B. G. (2017). Scene based non-uniformity correction for optical remote sensing imagery. *International Journal of Image, Graphics and Signal Processing, 9*(12), 50–57. https://doi.org/10.5815/IJIGSP.2017.12.06
7. Guang, J., Xue, Y., Fan, C., Li, Y., She, L., Che, Y. (2016). Estimate the high-resolution distribution of ground-level particulate matter based on space observations and a physical-based model. Published in: *2016 IEEE International Geoscience and Remote Sensing Symposium (IGARSS)*, 4211–4214. https://doi.org/10.1109/IGARSS.2016.7730097
8. Gupta, P., Christopher, S. A. (2009). Particulate matter air quality assessment using integrated surface, satellite, and meteorological products: Multiple regression approach. *Journal of Geophysical Research: Atmospheres, 114*(D14), D14205. https://doi.org/10.1029/2008JD011496
9. Harusi, N. M. R., Aly, S. H., Mitani, Y., Fauzan, M., Amru, K. (2025). Seasonal Estimation of NO2 Concentrations Using Land Surface Temperature from Landsat 8 and MODIS Imagery in Makassar Metropolitan City. *International Journal on Advanced Science, Engineering and Information Technology*, *15*(6), 1872–1881. https://doi.org/10.18517/ijaseit.15.6.21694
10. Han, S., Sun, B., Zhang, T. (2020). Mono- and polycentric urban spatial structure and PM2.5 concentrations: Regarding the dependence on population density. *Habitat International, 104*, 102257. https://doi.org/10.1016/J.HABITATINT.2020.102257
11. Heriza, D., Wu, C. D., Syariz, M. A., Lin, C.-H. (2023). Analysis of spatial-temporal variability of PM2.5 concentrations using optical satellite images and geographic information system. *Remote Sensing, 15*(8), 2009–2009. https://doi.org/10.3390/rs15082009
12. IQAir. (2024). Kualitas Udara di Sulawesi Selatan. https://www.iqair.com/id/indonesia/southsulawesi?srsltid=AfmBOor3osaOM4QrhQ7s1KDxi9obqDf3zy9NBO9PWMyh4hVgiGQa0bM
13. Irawadi, R., Razif, M. (2023). Keterkaitan curah hujan terhadap PM2.5 dan PM10 di Pos Pengamatan Kualitas Udara Cibereum, Bogor. *Envirotek: Jurnal Ilmiah Teknik Lingkungan, 15*(1), 22–26. https://doi.org/10.33005/envirotek.v15i1.216
14. Kumar, P., Gurjar, B. R., Nagpure, A. S., Harrison, R. M. (2011). Preliminary estimates of nanoparticle number emissions from road vehicles in megacity Delhi and associated health impacts. *Environmental Science & Technology, 45*(13), 5514–5521. https://doi.org/10.1021/es2003183
15. Kementerian Lingkungan Hidup dan Kehutanan Republik Indonesia (KLHK). (2023). Status mutu udara ambien Indonesia tahun 2023. https://www.menlhk.go.id/
16. Lin, H., Lin, H., Li, S., Xing, J., He, T., Yang, J., Wang, Q. (2021). High resolution aerosol optical depth retrieval over urban areas from Landsat-8 OLI images. *Atmospheric Environment, 261*, 118591. https://doi.org/10.1016/J.ATMOSENV.2021.118591
17. Liu, S., Wang, S. (2024). Fine-scale mapping of particulate matter using landsat imagery and low-cost sensor data from Purpleair: A case study of Los Angeles. *IGARSS 2024 - 2024 IEEE International Geoscience and Remote Sensing Symposium* 3850–3853. https://doi.org/10.1109/igarss53475.2024.10642252
18. Loew, A., Bell, W., Brocca, L., Bulgin, C. E., Burdanowitz, J., Calbet, X., Donner, R. V., Ghent, D., Gruber, A., Kaminski, T., Kinzel, J. (2017). Validation practices for satellite-based Earth observation data across communities. *Reviews of Geophysics, 55*(3), 779–817. https://doi.org/10.1002/2017RG000562
19. Othman, N., Jafri, M. Z. M., San, L. H. (2010). Estimating particulate matter concentration over arid region using satellite remote sensing: A case study in Makkah, Saudi Arabia. *Modern Applied Science, 4*(11), 131. https://doi.org/10.5539/mas.v4n11p131
20. Phan, C. C., Nguyen, T. Q. H., Nguyen, M. K., Park, K., Bae, G.-N., Seung-bok, L., Bach, Q.-V. (2020). Aerosol mass and major composition characterization of ambient air in Ho Chi Minh City, Vietnam. *International Journal of Environmental Science and Technology, 17*(6), 3189–3198. https://doi.org/10.1007/S13762-020-02640-0
21. Putri, J. F., Bioresita, F. (2024). Pengamatan persebaran konsentrasi polutan udara (termasuk PM10) dengan citra Landsat 8 di Jawa Tengah (2019–2022). *Elipsoida: Jurnal Geodesi dan Geomatika.* https://ejournal2.undip.ac.id/index.php/elipsoida/article/view/24167
22. Ranjan, A. K., Patra, A. K., Gorai, A. Kr. (2021). A Review on estimation of particulate matter from satellite-based aerosol optical depth: Data, methods, and challenges. *Asia-Pacific Journal of Atmospheric Sciences, 57*(3), 679–699. https://doi.org/10.1007/S13143-020-00215-0
23. Salsabila, P. H., Aly, S. H., Hustim, M., Masyiah, N., Harusi, R., Azizah, A., Dinanti, N., Pala, H. (2026). *Satellite-based estimation and ground validation of air pollutants in a cement industry area in Indonesia*. *27*(2), 457–473.

24. Santoso, M., Hopke, P. K., Permadi, D. A., Damastuti, E., Lestiani, D. D., Kurniawati, S., Khoerotunnisya, D., Sukir, S. K. (2021). Multiple air quality monitoring evidence of the impacts of large-scale social restrictions during the COVID-19 pandemic in Jakarta, Indonesia. *Aerosol and Air Quality Research, 21*(8), 200645. https://doi.org/10.4209/AAQR.200645
25. Saraswat, I., Mishra, R. K., Kumar, A. (2017). Estimation of PM10 concentration from Landsat 8 OLI satellite imagery over Delhi, India. *Remote Sensing Applications: Society and Environment, 8*, 251–257. https://doi.org/10.1016/j.rsase.2017.10.006
26. Shaddick, G., Thomas, M. L., Mudu, P., Ruggeri, G., Gumy, S. (2020). Half the world's population are exposed to increasing air pollution. *npj Climate and Atmospheric Science 3*(1), 1–5. https://doi.org/10.1038/S41612-020-0124-2
27. Small, C., Zappa, C. J. (2017). Mapping the diurnal thermal response of the urban heat island with Landsat TIRS. *2017 Joint Urban Remote Sensing Event (JURSE),* 1–4. https://doi.org/10.1109/JURSE.2017.7924532
28. Thanvisitthpon, N., Kallawicha, K., Chao, H. (2024). Effects of urbanization and industrialization on air quality. *Health and Environmental Effects of Ambient Air Pollution,* 231–255. https://doi.org/10.1016/b978-0-443-16088-2.00003-x
29. Usman, M. (2023). PM2.5 concentration pattern in ASEAN countries based on population density. *Procedia of Engineering and Life Science, 4*. https://doi.org/10.21070/pels.v4i0.1385
30. World Health Organization. (2021). *WHO global air quality guidelines: Particulate matter (PM2.5 and PM10), ozone, nitrogen dioxide, sulfur dioxide and carbon monoxide*. World Health Organization. https://iris.who.int/handle/10665/345329
31. Yang, Y., Chen, Y., Yang, K., Chen, Y., Sun, Y., Yang, D. (2021). A new aerosol retrieval algorithm for Landsat 8 OLI images over urban areas. *2021 IEEE International Geoscience and Remote Sensing Symposium IGARSS*, 7208–7211. https://doi.org/10.1109/IGARSS47720.2021.9553612
32. Zaman, N. A. F. K., Kanniah, K. D., Kaskaoutis, D. G. (2017). Estimating particulate matter using satellite based aerosol optical depth and meteorological variables in Malaysia. *Atmospheric Research, 193*, 142–162. https://doi.org/10.1016/j.atmosres.2017.04.019
33. Zhang, B., Zhang, M., Kang, J., Hong, D., Xu, J., Zhu, X. X. (2019). Estimation of PMx concentrations from Landsat 8 OLI images based on a multilayer perceptron neural network. *Remote Sensing, 11*(6), 646. https://doi.org/10.3390/RS11060646